Atomic configurations of Au-induced nanowires on Ge(001) stabilized by higher Au coverages

K. Seino* and F. Bechstedt

Institut für Festkörpertheorie und-optik, Friedrich-Schiller-Universität Jena, Max-Wien-Platz 1, 07743 Jena, Germany

(Received 2 December 2015; revised manuscript received 11 February 2016; published 4 March 2016)

Based on density functional calculations with different exchange-correlation functionals we propose three new atomic structures for gold-induced nanowires on Ge(001) surfaces for Au coverages higher than one monolayer. We start the investigations from the original and a modified giant missing row (GMR) structure, the Au-trimer stabilized Ge ridge model. We replace successively Ge atoms at the wire ridge or facets by Au ones. Comparing the relative formation energies the new models are shown to be energetically more favorable than the GMR model proposed previously for lower coverages. Indeed, additional Au atoms at the wire surface stabilize novel geometries. The new models are able to explain several features of the nanowire structure observed by scanning tunneling microscopy and the electronic states found experimentally by angle-resolved photoemission spectroscopy.

DOI: 10.1103/PhysRevB.93.125406

I. INTRODUCTION

One-dimensional (1D) electronic systems have attracted much interest, because of fundamental problems as well as technological reasons. Self-organized arrays of atomic chains due to metal adsorption on semiconductor surfaces offer a variety of tunable model systems to study exotic physics but also novel applications in a nearly 1D situation. In addition, they are in focus as systems to test predictions from solid-state theory. They pertain to the Peierls instability of such chains, where a charge-density wave (or even a spin-density wave) leads to a metal-semiconductor transition [1]. For strictly 1D systems, the Fermi-liquid picture breaks down. A correlated electron state with spin-charge separation known as the Luttinger liquid is proposed [2]. Prototypical systems are In chains on Si(111) [3–5], Au on Si(111), Si(557), and Si(553) [6–8], and Pt on Ge(001) [9–13] (see also references therein).

Self-assembled nanowires have been also observed for Au on Ge(001) [12,14–26]. These nanowires have attracted much attention because they are candidate systems for observation of a Tomonaga-Luttinger liquid [15]. Indeed, on the basis of measurements of scanning tunneling spectroscopy and angle-resolved photoemission spectroscopy (ARPES) Blumenstein *et al.* [21] claimed that the observed density of states is a clear hallmark of a Tomonaga-Luttinger liquid. This conclusion has been, however, controversially discussed in literature [26]. Central and most controversial points are the findings and interpretation of the ARPES but also scanning tunneling microscopy (STM) results concerning the metallic state, its one- or two-dimensionality, anisotropy, and dispersion [17,19,20,24–26].

In contrast to the electronic structure the surface morphology is consistently interpreted, mainly on the basis of STM images (sometimes supported by low-energy electron diffraction (LEED)) taken at low or room temperature [15,16,18,22,24,26]. The Au-induced chains grow in a $\langle 110 \rangle$ direction with a regular width and an interwire spacing of 1.6 nm, i.e., by four Ge(001)1 × 1 surface lattice constants a with $a = a_0/\sqrt{2} = 4.0$ Å (a_0 – bulk Ge lattice constant). Long-range order of the wire arrays was difficult to achieve and interpreted by the $c(8 \times 2)$ translational symmetry [15,21]. Now in well-ordered surface regions a further long-range ordering with a more complex superstructure is observed. It appears 4×8 unit cells with characteristically modulated protrusions along a wire, which are labeled as "*V* (chevron)" and "*W* (zigzag)" protrusions [18,22,24,26]. This superstructure on top of the $c(8 \times 2)$ unit cells may be more precisely described by a $\begin{pmatrix} 0 & -8 \\ 4 & 1 \end{pmatrix}$ superstructure matrix [22,24] using a generalized description of the surface translational symmetry [27]. Some groups claim now that the $c(8 \times 2)$ symmetry corresponds to a higher temperature phase [22] and reassigns the low-temperature phase as the $p(4 \times 1)$ superstructure of $c(8 \times 2)$ [21,25], which may be the same as the 4×8 structure [26].

Another not-well-defined characteristic of the Au/Ge(001) surface is the gold coverage measured in monolayers (MLs). In many experimental investigations an Au coverage of 0.5 or 0.75 ML has been found or assumed to interpret the results [15,19,26,28]. Recently, there is a tendency to interpret the ARPES and STM results even in terms of somewhat higher coverages, e.g., 0.96 ML [20], 1.1–1.2 ML [17], and 1.0 ML [25]. Very recent studies combining STM and transmission electron microscopy [29] or LEED [30] favor higher coverages with Au atoms penetrated into the Ge(001) surface. These results are in line with early reports of 1.5 ML Au coverages [14].

The experimental controversies concerning electronic structure, details of the surface topology, and surface stoichiometry make theoretical modeling far from trivial. Therefore, despite several atomic and electronic structure studies in the framework of the density functional theory (DFT) [12,31–34], the actual arrangements of the Au and Ge atoms at the Au/Ge(001) surface are almost unknown or, at least, under discussion [13]. The suggested surface models and their possible modifications can be roughly classified into four classes suggested by Sauer *et al.* [31] and Vanpoucke [13]. Among these classes the simulated STM images from the giant missing row (GMR) structure, at first suggested by van Houselt *et al.* [16], show relatively good agreement with the recent experimental STM images [18,22,24,26]. Moreover, one of

*seino@ifto.physik.uni-jena.de

the most recent LEED studies supports that the GMR model is most appropriate to describe the Au-induced nanowires on Ge(001) [30]. The replacement of Ge dimers on the wire ridge of the GMR model by Ge-Au heterodimers leads to a Au-trimer stabilized Ge ridge (ATSGR) structure, which is much more energetically stable than the original GMR model [31]. Therefore, further developments of structural models for higher coverage may be started from the ATSGR structure.

In this paper, we investigate new possible atomic models for Au-induced nanowires on the Ge(001) surface for higher Au coverage by means of first-principles calculations. We focus on the influence of the surface stoichiometry on the stability of a certain wire model. We report on the electronic properties of these new models and discuss the results in terms of available experimental data.

II. THEORETICAL AND COMPUTATIONAL METHODS

The total-energy and electronic-structure calculations are performed in the framework of the DFT [35,36] within the local density approximation (LDA) as well as the generalized gradient approximation (GGA) introduced by Perdew, Burke, and Ernzerhof (PBE) [37,38] using the Vienna *ab initio* simulation package (VASP) implementation [39]. From previous calculations [31] we know that neither the LDA nor the GGA lead to reasonable results simultaneously for the lattice constants and cohesive energies of bulk gold and the group-IV crystals. The theoretical lattice constants underestimate the experimental values for LDA or overestimate them for PBE-GGA. Therefore, here we also test a modern GGA functional, PBEsol [40], intended only for solid and surface systems. We use a plane-wave basis and projector-augmented wave pseudopotentials [41]. The electronic wave functions are expanded into plane waves up to an energy cutoff of 400 eV. The outermost s, p, and d electrons are treated as valence electrons.

The gold-covered Ge(001) surface is modeled with a periodically repeated slab. The supercells consist of eight Ge layers, additional Ge and Au atoms simulating the wire, and a vacuum thickness of 16–20 Å. The numbers of the additional atoms determine the Ge content of the wires and the Au coverage (see Ref. [31]). The bottom layer of the slab is saturated with hydrogen atoms. Eight Ge layers together with H-termination of lower slab side are used to model bulk germanium. They correspond to four irreducible (001) slabs of the diamond structure [27]. This material slab has been tested to be thick enough for energy and structural calculations [31]. The wires on the Ge(001) surface are simulated by further six or seven Au/Ge atomic layer.

All calculations are performed using the calculated Ge equilibrium bulk lattice constant for each exchange-correlation (XC) functional. The calculations yield a lattice constant of $a_0 = 5.65$, 5.78, and 5.70 Å for bulk Ge from the LDA, PBE-GGA, and PBEsol XC functionals, respectively. These values are in good agreement with previous calculations [13,31,42]. We investigate unit cells with $c(8 \times 2)$ and $p(4 \times 2)$ surface translational symmetries. The $p(4 \times 2)$ structure has been suggested alternatively to the $c(8 \times 2)$ one. Although a 4×8 unit cell is reported from the STM experiment recently [26], the $c(8 \times 2)$ and $p(4 \times 2)$ unit cells represent basic symmetries of the 4×8 periodicity. Nevertheless, a few electronic structure calculations are performed for the $p(4 \times 4)$ unit cells, which are of the double size of the $c(8 \times 2)$ and $p(4 \times 2)$ unit cells. The Brillouin zone (BZ) integrations are performed using Monkhorst-Pack meshes [43] of $3 \times 3 \times 1$ for $c(8 \times 2)$, $2 \times 4 \times 1$ for $p(4 \times 2)$, and $10 \times 10 \times 10$ ($20 \times 20 \times 20$) in the case of bulk Ge (Au), respectively. The topmost five atomic layers of the slab are allowed to relax until the Hellmann-Feynman forces are less than 10 meV/Å.

The resulting electronic structures based on the Kohn-Sham eigenvalues of the DFT [36] suffer from the neglect of the quasiparticle excitation aspect [44]. The quasiparticle gap opening is of the order of the fundamental gap itself [45]. However, a second problem exists in the case of germanium in diamond geometry. In the framework of the PBE-GGA or LDA XC functional the semiconductor becomes direct with a vanishing gap and a small indirect gap [46]. Converged quasiparticle calculation using the *GW* self-energy cannot be performed for supercells with about 100 or 200 atoms [44]. Also approximate quasiparticle approaches, e.g., using the MBJLDA functional cannot be performed because of strongly inhomogenous system containing of vacuum, surface region and bulk layers [46]. Fortunately, the slab approximation has an influence on the actual gap in the electronic structure. The confinement effects in normal direction open a small gap mainly determined by $\hbar^2(\pi/d_{\mathrm{slab}})^2/2m^*$, where m^* is an effective electron mass and d_{slab} is a slab thickness. With an electron mass of the order of $m^* = 0.5m$ and a (bulk) slab thickness of about $d_{\mathrm{slab}} = 12$–20 Å the confinement leads to a gap opening of approximately 0.2–0.5 eV. This fact helps to discuss surface and wire electronic states in the gap region of "bulk" Ge.

In order to compare the energies of models with different Au and Ge coverages, i.e., different number of atoms in unit cells, we compute the relative formation energies by $\Delta\Omega_f = E_{\mathrm{slab}} - E^{\mathrm{ref}}_{\mathrm{slab}} - \mu_{\mathrm{Ge}}\Delta N_{\mathrm{Ge}} - \mu_{\mathrm{Au}}\Delta N_{\mathrm{Au}}$ with E_{slab} as the total energy of the slab, μ_{Ge} (μ_{Au}) as the chemical potential of Ge (Au), and ΔN_{Ge} (ΔN_{Au}) as the variation of the number of Ge (Au) atoms with respect to the reference model. In all practical cases, we compare with the GMR model [31] as a reference surface. The chemical potentials μ_{Ge} (μ_{Au}) are referred to the calculated bulk chemical potentials $\mu^{\mathrm{bulk}}_{\mathrm{Ge}}$ ($\mu^{\mathrm{bulk}}_{\mathrm{Au}}$) for the specified atoms. They allow to study fluctuations $\Delta\mu_{\mathrm{Ge(Au)}} = \mu_{\mathrm{Ge(Au)}} - \mu^{\mathrm{bulk}}_{\mathrm{Ge(Au)}}$.

III. RESULTS AND DISCUSSIONS

A. Structural models

We introduce three new models for Au-induced nanowires on Ge(001). The starting point of the first one is the ATSGR model, which was proposed in a previous DFT study by Sauer *et al.* [31] shown in Fig. 1(a). This model is the most stable atomic structure among the GMR class with not too high Au coverage. In order to seek possible atomic structures for Au-induced nanowires on Ge(001) we first studied modifications from the ATSGR model. We replaced two or four Ge atoms by Au atoms in the surface region of the ATSGR model, thereby increasing the Au coverage. The Au coverage became 1.0 and 1.25 ML, respectively. However, we did not find structures with an actually better energetic stability under Au-rich preparation

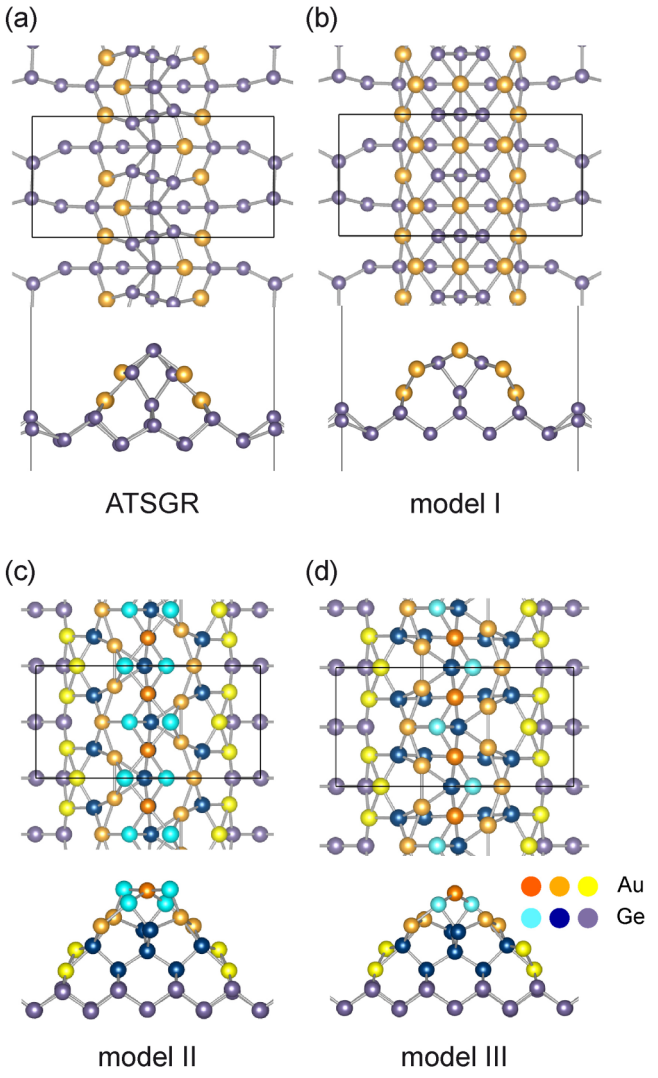

FIG. 1. Calculated atomic structures (top view and side view) of the (a) ATSGR structure, (b) model I, (c) model II, and (d) model III using the PBE-GGA XC functional.

conditions. For that reason, we modified the idea for a new model based on the ATSGR model. In a first step we add two Au atoms on the ATSGR structure resulting in Θ_{Au}=1.0 ML. In a second step we replace two Ge atoms by two Au atoms on the surface. The resulting stable structure shown in Fig. 1(b), "model I," gave rise to an improvement of the energy gain under Au-rich conditions, at least within PBE-GGA, as shown in Table I. In this model I the entire surface reconstruction in $p(4 \times 2)$ unit cells contains 1.25 ML of Au atoms.

The model I in Fig. 1(b) shows two characteristic features, a half-cylinder form of the wire and deep grooves around it. More in detail, a linear chain of Au atoms at the wire apex is constructed, instead of a linear chain of Ge atoms in the case of the ATSGR structure. Consequently, the atomic structure of model I has no more Ge homodimers or Ge-Au heterodimers on top of the ridge. Four Au atoms on each facet side are observed on the nanowires. Thereby, the atomic geometry of the nanowire is symmetric. Buckled Ge dimers are still formed in the trenches, similar to the original ATSGR model shown in Fig. 1(a).

TABLE I. Relative formation energies $\Delta\Omega_f$ in eV per $p(4 \times 2)$ unit cell of the GMR, ATSGR, and new proposed models derived for three different exchange-correlation functionals. The related formation energies are relative to the GMR model. The Au coverage Θ_{Au} is given in monolayer (ML). Au-rich preparation conditions $\mu_{\mathrm{Au}} = \mu_{\mathrm{Au}}^{\mathrm{bulk}}$ are assumed.

Model	Θ_{Au}	LDA	PBE-GGA	PBEsol
GMR	1.0	0.00	0.00	0.00
ATSGR	0.75	−3.18	−1.99	−2.95
Model I	1.25	−2.73	−2.29	−2.65
Model II	1.75	−2.49	−2.35	−2.52
Model III	1.75	−2.06	−2.33	−2.18

The interpretation of x-ray photoemission spectroscopy results [18] claims that buckled Ge dimers do not occur. For that reason, we construct another geometry, which has no buckled Ge dimers in the trenches. We go back to the original unfavorable GMR model [31] but consider a combination of the GMR model and the wire shape of the half-cylinder form found for model I by adding Au atoms to reach a Au coverage of 1.75 ML. Figure 1(c) shows the resulting atomic structure. We call this model "model II" hereafter. In order to understand better model II in Fig. 1(c) we use different colors for Au and Ge atoms to illustrate different heights above the grooves. Mixed elements consisting of Ge and Au atoms are contained in the top layer of model II. Au trimers, which are displayed as yellow balls in Fig. 1(c), are constructed on the facets. The Au-Ge bond lengths between the topmost Au atoms [dark orange balls in Fig. 1(c)] and Ge atoms [light blue balls in Fig. 1(c)] are 2.60–2.78 Å. The Au atoms in the middle position on the facets [light orange balls in Fig. 1(c)] represent Au-Au pairs, in which the Au-Au distances are 2.91 and 2.97 Å within PBE-GGA, close to the Au-Au bond length 2.95 Å of fcc bulk Au. Interestingly, the model II has a slightly lower formation energy than the model I within PBE-GGA and a somewhat higher formation energy than the model I in LDA and PBEsol for Au-rich preparation conditions, i.e., $\mu_{\mathrm{Au}} = \mu_{\mathrm{Au}}^{\mathrm{bulk}}$, as shown in Table I. The difference in the formation energies are mainly due to the different cohesive energies of bulk Au and Ge resulting for the different XC functionals [13,31].

We also discuss a modification of model II, because the distribution of the Ge atoms on the top of the nanowires [light blue balls in Fig. 1(c)] seems to be somewhat too dense. In order to remove a few Ge atoms at the ridge in the $p(4 \times 2)$ unit cells and reconstruct the atomic structure, we propose the third variation of the nanostructure of Au-induced nanowires on a Ge(001) surface, "model III," shown in Fig. 1(d). The Au coverage between models II and III remains same. Both models have a Au coverage of 1.75 ML. However, the number of Ge atoms is different between models II and III because two Ge atoms have been taken away from ridge of model II. A zigzag structure based on topmost Au atoms [bright orange balls in Fig. 1(d)] and Ge atoms [light blue balls in Fig. 1(d)] results at the apex of the ridge. The Au-Ge distance in the zigzag lines is 2.52 Å. Two Au dimers in the direction of the chain appear under the Au-Ge zigzag chain in model III. The characteristic lengths as obtained in PBE-GGA are 2.84 Å, which are smaller

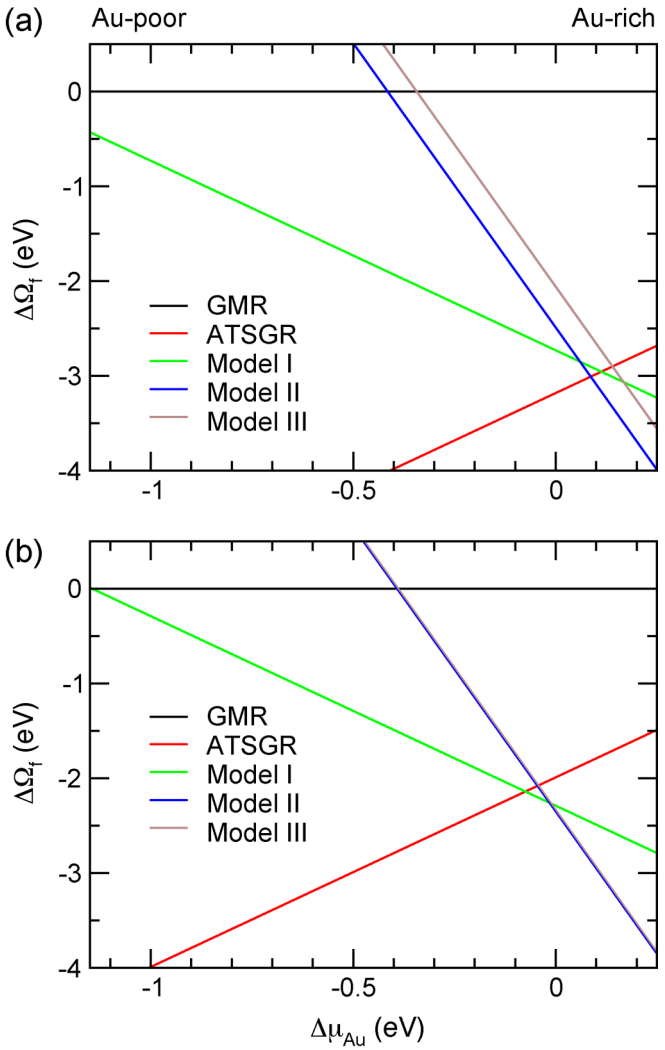

FIG. 2. Relative formation energies of Au/Ge(001) $p(4 \times 2)$ surfaces $\Delta\Omega_f$ in eV per $p(4 \times 2)$ unit cell versus the fluctuation of the chemical potential of Au atoms μ_{Au} calculated within (a) LDA and (b) PBE-GGA.

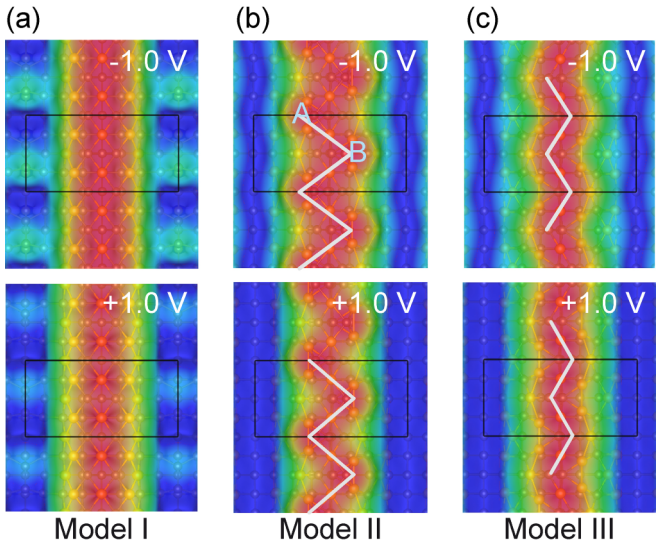

FIG. 3. Simulated STM images for the (a) model I, (b) model II, and (c) model III for occupied (−1.0 V) and empty (+1.0 V) states. The bright (red) regions describe protrusions while dark (blue) regions indicate deep corrugations. The black solid lines indicate $p(4 \times 2)$ unit cells. To guide the eyes "W" shapes are displayed on the wire top.

than the Au-Au distances for the corresponding Au-Au pairs in model II. Model III is also energetically much more favorable than the GMR structure but also the ATSGR model (at least within PBE-GGA) as shown in Table I. The model III also has no buckled Ge dimers (in agreement with Ref. [18]) and the Au trimers still remain on the side facets shown by the yellow balls in Fig. 1(d).

The stability of the studied five surface models for varying preparation conditions is characterized by the phase diagram in Fig. 2. Independent of the XC functionals used in the total-energy calculations it shows that under Au-rich preparation conditions the ATSGR model and models I, II, and III derived from the original GMR model and the ATSGR structure possess a similar energetic stability for both LDA and PBE-GGA XC functionals. However, toward Au-poor preparation conditions the ATSGR model is clearly favored. Therefore, we claim that contradictory spectroscopic results [20,21,26], for example, for the dimensionality of surface bands, may be traced back to different surface preparations.

B. STM images

In order to simulate the STM images we apply the Tersoff-Hamann scheme [47]. Since the STM measurements are usually performed within the constant current mode, we apply the implementation of this mode in VASP by Sauer *et al.* [31]. We calculate filled- and empty-state images for a bias voltage of −1.0 V and +1.0 V, respectively, with the PBE-GGA XC functional. These voltages correspond to integration intervals in the Kohn-Sham band structures of a length of 1.0 eV from the Fermi energy into the occupied or empty states. The STM images resulting for the new models I, II, and III are presented in Fig. 3. In general, all images show wire structures with varying width and structural details but arrays of wires separated by 1.6 nm in accordance with the experimental findings [15,16,18,21,22,24,26]. The wire widths (given by red and yellow regions) of somewhat less the half wire distances also agree with the experimental findings for not too small bias voltages.

We investigate the resulting images especially concerning the appearance of the characteristically modulated protrusions along a wire, which are of the "V (chevron)" or "W (zigzag)" type [18,22,24,26]. For model I, the simulated STM images at a bias of −1.0 V or +1.0 V obtained from Fig. 3(a) show almost straight lines along the chain direction. Therefore, the model I cannot explain a zigzag feature with a V or W form. That means, neither the original ATSGR structure [31], nor the modified one, model I with a higher Au coverage, describes the zigzag chains in the STM images found experimentally. We state a clear contradiction between their lower relative formation energies in Table I under Au-rich preparation conditions and the accompanying STM images of the filled and empty states with experimental findings.

For model II the simulated STM images within $p(4 \times 2)$ unit cells are shown in Fig. 3(b). For this model the filled-state

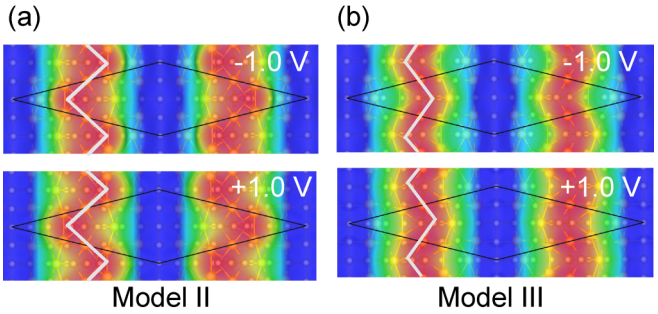

FIG. 4. Simulated STM images within $c(8 \times 2)$ unit cells (black solid lines) for (a) model II and (b) model III. To guide the eyes "W" shapes are displayed on the wire top.

and empty-state images show bright spots at one side of the nanowires for $2\times$ periodicity in the chain direction for the both occupied and unoccupied states. At the opposite side of the chains the corresponding spots are less pronounced. The zigzag chains in the simulated STM images for model II are generated by Ge atoms bonded with the Au-Au pairs. Nevertheless, the model II can be interpreted as the configuration leading to W-like zigzag features observed for both filled- and empty-state images.

The calculated STM image at a bias of -1.0 V also shows a zigzag chain for model III as depicted in Fig. 3(c). The zigzag feature is less pronounced than the STM image simulated for the model II. In particular, the width of the zigzag line for model III is smaller than the image from model II. Nevertheless, the resulting zigzag feature may also explain the W-type zigzag images found in STM experiments [18,22,24,26]. The topmost Ge atoms [light blue balls in Fig. 1(d)] construct local zigzag structures in the simulated STM. Therefore, the zigzag structures between models II and III have a phase shift. However, the width of a zigzag line in the empty-state image is somewhat smaller than that in the filled-state image. The nanowire edges show almost a straight behavior in the simulated filled-state STM image. The reason seems to be the influence of the topmost Au atoms [dark orange balls in Fig. 1(d)]. In any case, the STM studies suggest that characteristic STM features, the W-shaped ones, can be generated within models II and III derived from the GMR model for high Au coverages, here a Au coverage of 1.75 ML. In contrast, the model I only show straight quantum wires similar to the original ATSGR model [31].

We have to mention that the chain structure with W-elements but adjacent wires displaced by half of a $2\times$ periodicity can be easily generated within the $c(8 \times 2)$ symmetry as demonstrated in Fig. 4. The relative formation energies within PBE-GGA are still of the order of magnitude of those for the $p(4 \times 2)$ translational symmetry (see Table I), -1.96 and -1.91 eV per $p(4 \times 2)$ unit cell. This fact suggests that mirror-symmetry combinations of models II or III in one wire and their staggered arrangement within the $c(8 \times 2)$ translational symmetry may lead to structures with similar energetical stability as found for the isolated elements within the $p(4 \times 2)$ translational symmetry. Indeed, the STM images obtained within $c(8 \times 2)$ cells in Figs. 4(a) and 4(b) show similar characteristic features as those within $p(4 \times 2)$ symmetry shown in Figs. 3(b) and 3(c).

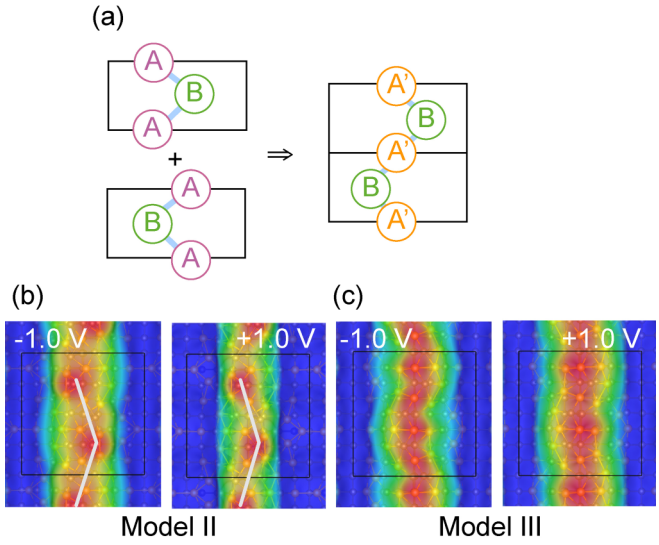

FIG. 5. (a) Combination of the STM spots of model II in a mirror symmetric way along the wires (schematic). The labels "A" and "B" denote spot positions in Fig. 3(b). Simulated STM images within $p(4 \times 4)$ unit cells (black solid lines) for (b) model II and (c) model III. In panel (b) the eyes are guided by a "V."

Based on model II, a V-like chain with $4a$ periodicity (a is the surface lattice constant) can be also generated if chain pieces are displaced by half of a unit cell and combined as illustrated in Fig. 5(a). In agreement with the observed long-range order discussed above the translational symmetry in wire direction may be doubled. In the simulation we go one step further. We consider a $p(4 \times 4)$ symmetry in order to combine two basic elements from the original atomic models II and III with a mirror symmetry element as illustrated in Fig. 5(a). If the bright spot "A" in Fig. 3(b) shifts to the center of the chain [A′ in the right panel of Fig. 5(a)], one gets a V-like chain, A′-B-A′-B-A′, in Fig. 5(a). Before the simulation of the STM images, we recalculated the atomic structures of models II and III within a $p(4 \times 4)$ symmetry. The model II within $p(4 \times 4)$ translational symmetry is energetically favorable. It has the formation energy of -2.00 eV/$p(4 \times 2)$ in the PBE-GGA framework. The calculated STM images for model II with a $p(4 \times 4)$ symmetry are shown in Fig. 5(b). Clear V-like features appear for the chains with $4a$ symmetry in the wire direction for both the negative and positive voltages. For model III we find less pronounced V-type zigzag images as reported by the experiments, as shown in Fig. 5(c). The formation energy, -1.48 eV/$p(4 \times 2)$, for model III within a $p(4 \times 4)$ translational symmetry also indicates that a combination of wire elements with mirror symmetry is energetically less favorable in the case of model III, in contrast to the findings for model II.

C. Electronic structures

The slab band structures of the three models I, II, and III are plotted versus high-symmetry lines in the BZ of the $p(4 \times 2)$ surface shown in Fig. 6(a) together with the resulting density of states (DOS). The calculations for electronic structures were done using the XC functional treated in PBE-GGA. The band structure of the model I clearly indicates a strongly

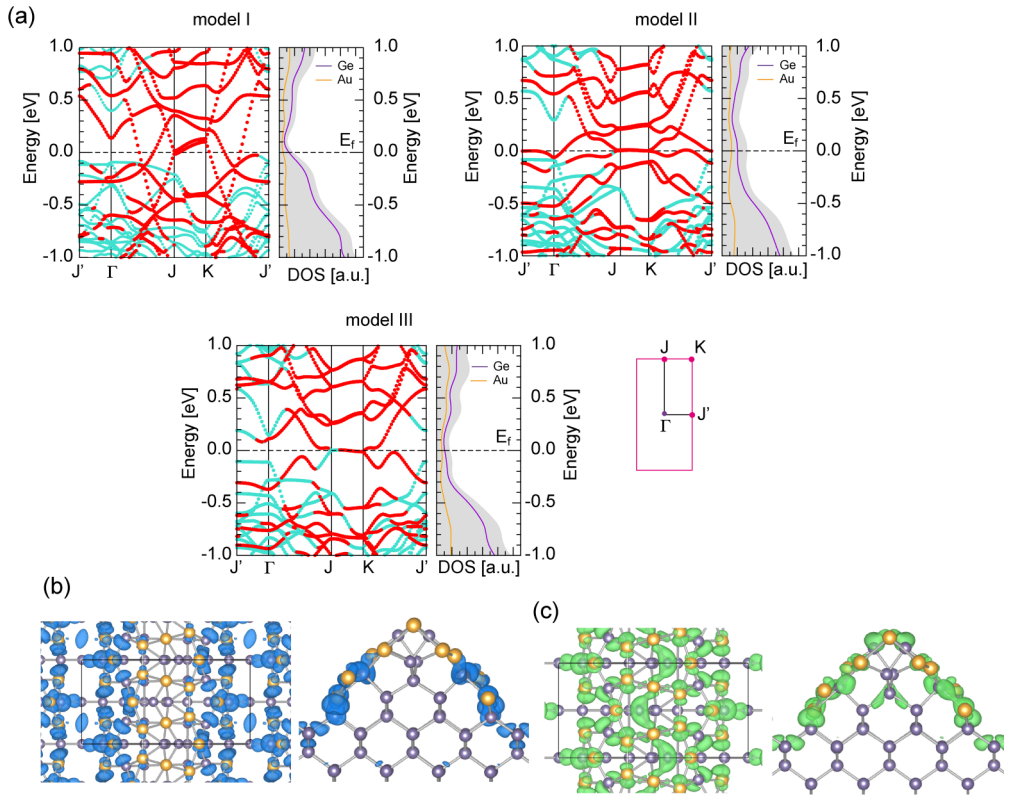

FIG. 6. (a) Electronic band structures and density of states (DOS) of the three proposed models I, II, and III versus the $p(4 \times 2)$ BZ. In the calculated bands, the red dots indicate states with strong contributions from Au and/or Ge atoms from the surface region. The blue dots indicate mainly Ge-bulk-related states. The Fermi energy is taken as energy zero. Shaded areas in the DOS plots represent the total DOS for each slab arrangement. The projected DOS on Ge (Au) atoms is indicated by a solid purple (orange) line. To illustrate the character of the band states the wave function squares of the states near the Fermi energy for the model III at the center of the J-K line ($0.5JK$) (b) for the lower flat band and (c) for the corresponding higher flat band are also given. Top and side views are displayed.

metallic surface with dispersive bands also in the J'-Γ and J-K directions perpendicular to the chains. The slab band structures, in general, indicate a much stronger 1D character in the case of the GMR-derived geometries, models II and III, in comparison to the ATSGR-derived model I. Along the J-K line the bands for models II and III are more flat indicating a 1D character. Such bands even pin the Fermi level. In the case of model I also the bands perpendicular to the wire direction exhibit a remarkable dispersion, indicating more a two-dimensional character. Along the J'-Γ line, also parallel to the chains, a gap is opened within all three models. Figure 6 illustrates that the details of the electronic structure of the wire as well as their stoichiometry strongly influence the band structure. On the other hand, main features of the DOS shown in Fig. 6 are similar among all models. Only small differences are found near the Fermi level.

A further general feature is the decrease of the metallicity of the Au-rich surface geometries along the nanowire models I, II, and III. The number of band crossings with the Fermi level decreases along this line. Finally, in model III the Fermi level is only passed by flat bands, whose wire character is investigated in Figs. 6(b) and 6(c). In the case of model III, the geometry gives rise to a fundamental gap apart from the BZ region near the J-K boundary. This is in contrast to model II. Pronounced parabolic surface bands near a $k_\parallel$-vector parallel to the wire with a minimum close to $k_\parallel = 0.2$ Å^{-1} [19] are not visible somewhat below the Fermi level. Such occupied parabolic bands are only observable near $0.75\Gamma J$ and $0.24KJ'$ along the chains using the $p(4 \times 2)$ BZ for model III shown in Fig. 6(a).

Figures 6(b) and 6(c) exhibit the probability of finding an electron or hole near the Fermi level for model III with a wave vector $0.5JK$ parallel to the wire direction. The hole wave functions for the lower flat band in Fig. 6(b) are localized at the lower parts of the facets at both wire sides. The wave functions of the electrons with the wave vector $0.5JK$ show a higher probability to find them closer to surface atoms for the other flat band in Fig. 6(c). Therefore, the Bloch states belonging to the two flat bands clearly demonstrate features of 1D physics.

For a better comparison with ARPES data and, hence, photoelectron k-space mapping we have recalculated the electronic band structures of the proposed new models II and III within $c(8 \times 2)$ unit cells. The resulting bands are plotted in Figs. 7(a) and 7(b) along high-symmetry lines within the surface BZ parallel ($\bar{\Gamma}$-$\bar{Y}'$ and $\bar{Y}'$-$\bar{J}$) and perpendicular ($\bar{J}$-$\bar{\Gamma}$) to the chains in a relatively small energy interval around and below the theoretical Fermi level. In Fig. 7(c) the surface $c(8 \times 2)$ BZ and its neighbors are displayed in the reciprocal space. Thereby, two different denotations of the high-symmetry points for c-rectangular or hexagonal lattices [27] are given. The red (blue) color of the dots indicates

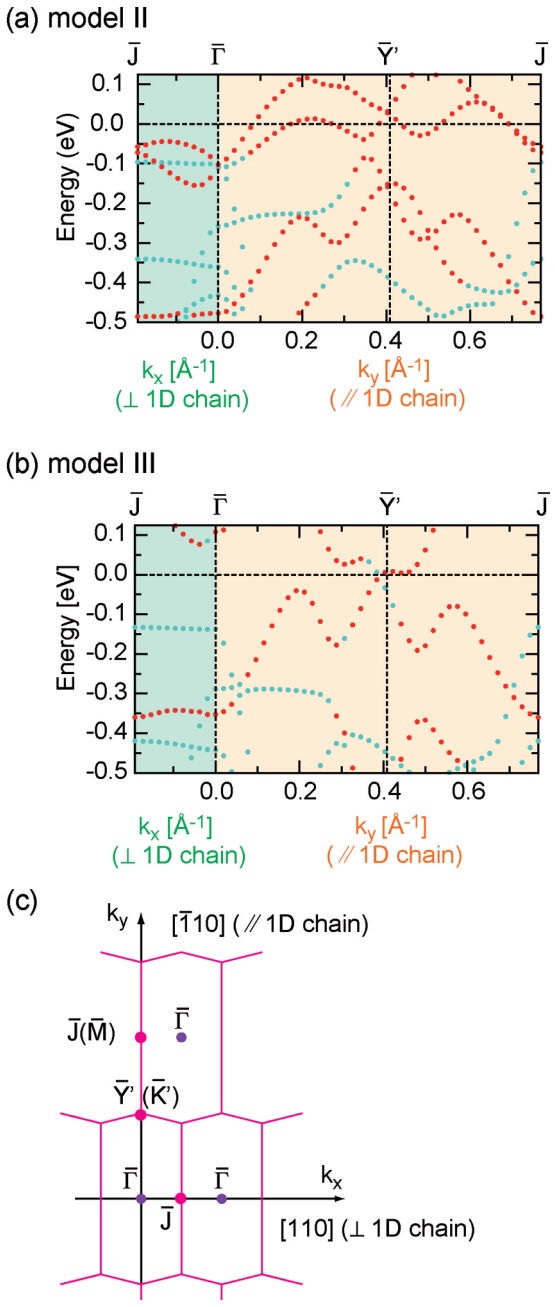

FIG. 7. Electronic band structures of (a) model II and (b) model III versus the $c(8 \times 2)$ BZ. The high-symmetry directions are explained in panel (c). The Fermi energy is taken as energy zero. In the calculated bands, the red dots indicate states with strong contributions from Au and/or Ge atoms from the surface region. The blue dots indicate mainly Ge-bulk related states. The red color characterizes that the wave functions are more than 50% localized in the wire regions [see Figs. 1(c) and 1(d)], whereas the blue ones show localization in the last two atomic layers of the wire and the remaining slab.

the almost wire (bulk) character of the corresponding band state. Only the band structures for models II and III are displayed, because within those geometries the majority of STM features could be explained.

Unfortunately, the ARPES measurements [17,19,20,25,48] do not give rise to a unique band structure picture, neither to the number of wire- and surface-related bands nor to their position in an energy-wave vector diagram. On the contrary, these facts are controversially discussed. This especially holds for the one- or two-dimensional character of the bands. Nevertheless, we claim that important features in these calculated bands can be related to experimental findings. One example is the surface-related bands crossed by or below the Fermi level along the $\bar{Y}'$-$\bar{J}$ line ($\bar{J}$-$\bar{K}$ line in Ref. [48]). In both models parabolic bands appear with minima at $\bar{J}$ and $0.20\bar{Y}'\bar{J}$, while the second minimum appears on the $\bar{J}\bar{K}$ axis in the measurements [48]. The binding energies of the two minima are underestimated (overestimated) in model II (III) compared to the experimental values of about -0.14 and -0.08 eV [48]. Moreover, in Ref. [48] the authors claim to observe band minima perpendicular to the chains, e.g., at $\bar{J}$. From this fact it is concluded that "the surface-state bands of Au/Ge(001) are obviously two dimensional." This conclusion is, however, not confirmed by the band structures in Figs. 7(a) and 7(b), despite the fact that model II exhibits surface bands with a binding energy of about -0.1 eV as in Refs. [20] and [48]. On the other hand, in two previous papers [17,20] of two of the authors only one parabolic, metallic band at $\bar{J}$ has been observed. In other ARPES measurements [19,25] only one 1D parabolic, metallic band has been observed along the wire direction with a band minimum at 0.2 Å^{-1} from the Γ point, i.e., near $0.5\bar{\Gamma}\bar{Y}'$. Such a band cannot be found in the calculated band structures. Only for model III such a pronounced band with similar binding energy of -0.18 eV in found but at a larger k_y value of about 0.29 Å^{-1} as shown in Fig. 7(b). Consequently, further experimental and theoretical studies are needed to derive a unified picture of the surface bands.

IV. SUMMARY AND CONCLUSIONS

We have studied the structural, energetic, and electronic properties of Au-induced nanowire arrays on Ge(001) surfaces by means of DFT calculations studying the $p(4 \times 2)$ but also $p(4 \times 4)$ and $c(8 \times 2)$ translational symmetries. Three new structures for a higher Au coverage in the range between 1.25 and 1.75 ML are proposed and compared with experimental results. The simulated STM images for all models reproduce the distance of 16 Å between atomic chains in agreement with the experimental STM results. We have explained both the V- and W-like chain features found experimentally in the simulated STM images by combinations of structural elements of models II and III based on a GMR-derived model for the first time. This finding is also important for understanding of the atomic configuration of long-range ordering seen in experimental low-temperature STM studies and their driving forces. For the GMR-derived models II and III we found a tendency for gap opening along the wire direction. In the case of model III, the weakest surface metallicity is found. Only flat bands perpendicular to the wire direction fix the Fermi level. Most interesting is that the new geometries with high Au coverages up to 1.75 ML show the same energetic stability for Au-rich preparation conditions as the ATSGR model. Especially in comparison with the original GMR model it becomes clear that higher Au coverages stabilize the wire system. Thereby, the influence of the chosen XC functional is weak but present.

The obtained results allow clear conclusions:

(i) Under gold-rich preparation conditions higher Au coverages are possible. This has been clearly demonstrated for modifications of the original GMR and ATSGR models by additional Au atoms on the wire ridges and sides or Au-Ge exchange reactions.

(ii) The almost similar formation energies suggest that different atomic geometries may be realized in dependence on the actual but similar preparation conditions. Therefore, we will not exclude that different experimental groups have studied different wire stoichiometries and geometries, consequently different electronic structures.

(iii) The new models derived from the original GMR one allow for W-shaped STM features and, in combination with larger $p(4 \times 4)$ unit cells, for V-shaped STM features. These facts suggest that more Au atoms at the ridges and side facets of the wires are necessary to explain the STM images of the wire arrays in detail.

(iv) The wave-functions squares for electrons and holes are distributed over the wire ridges and/or sides. However, their interpretation as 1D features is not unique. The bands with wave vectors perpendicular to the wire direction show a weaker dispersion compared to wave vectors in wire direction. However, their dispersion depends on the contributing atoms and, hence, the overlap of wave functions from adjacent unit cells.

ACKNOWLEDGMENTS

We acknowledge financial support by the Deutsche Forschungsgemeinschaft through research units FOR 1700 (Grant No. Be1346/21-1). We thank J. Schäfer, F. Komori, and I. Mochizuki for valuable discussions.

[1] G. Grüner, *Density Waves In Solids (Frontiers in Physics)* (Addison-Wesley, MA, 1994).
[2] J. Voit, Rep. Prog. Phys. **58**, 977 (1995).
[3] A. A. Stekolnikov, K. Seino, F. Bechstedt, S. Wippermann, W. G. Schmidt, A. Calzolari, and M. Buongiorno Nardelli, Phys. Rev. Lett. **98**, 026105 (2007).
[4] S. Wippermann and W. G. Schmidt, Phys. Rev. Lett. **105**, 126102 (2010).
[5] H.-J. Kim and J.-H. Cho, Phys. Rev. Lett. **110**, 116801 (2013).
[6] P. C. Snijders and H. H. Weitering, Rev. Mod. Phys. **82**, 307 (2010).
[7] S. C. Erwin and F. J. Himpsel, Nat. Commun. **1**, 58 (2010).
[8] F. Hötzel, K. Seino, C. Huck, O. Skibbe, F. Bechstedt, and A. Pucci, Nano Lett. **15**, 4155 (2015).
[9] U. Schwingenschlögl and C. Schuster, Eur. Phys. J. B **60**, 409 (2007).
[10] A. A. Stekolnikov, F. Bechstedt, M. Wisniewski, J. Schäfer, and R. Claessen, Phys. Rev. Lett. **100**, 196101 (2008).
[11] U. Schwingenschlögl and C. Schuster, Euro. Phys. Lett. **81**, 26001 (2008).
[12] J. Schäfer, S. Meyer, C. Blumenstein, K. Roensch, R. Claessen, S. Mietke, M. Klinke, T. Podlich, R. Matzdorf, A. A. Stekolnikov, S. Sauer, and F. Bechstedt, New J. Phys. **11**, 125011 (2009).
[13] D. E. P. Vanpoucke, J. Phys.: Condens. Matter **26**, 133001 (2014).
[14] J. Wang, M. Li, and E. I. Altman, Phys. Rev. B **70**, 233312 (2004).
[15] J. Schäfer, C. Blumenstein, S. Meyer, M. Wisniewski, and R. Claessen, Phys. Rev. Lett. **101**, 236802 (2008).
[16] A. van Houselt, M. Fischer, B. Poelsema, and H. J. W. Zandvliet, Phys. Rev. B **78**, 233410 (2008).
[17] K. Nakatsuji, R. Niikura, Y. Shibata, M. Yamada, T. Iimori, and F. Komori, Phys. Rev. B **80**, 081406 (2009).
[18] R. Niikura, K. Nakatsuji, and F. Komori, Phys. Rev. B **83**, 035311 (2011).
[19] S. Meyer, J. Schäfer, C. Blumenstein, P. Höpfner, A. Bostwick, J. L. McChesney, E. Rotenberg, and R. Claessen, Phys. Rev. B **83**, 121411 (2011).
[20] K. Nakatsuji, Y. Motomura, R. Niikura, and F. Komori, Phys. Rev. B **84**, 115411 (2011).
[21] C. Blumenstein, J. Schäfer, S. Mietke, S. Meyer, A. Dollinger, M. Lochner, X. Y. Cui, L. Patthey, R. Matzdorf, and R. Claessen, Nat. Phys. **7**, 776 (2011).
[22] C. Blumenstein, J. Schäfer, M. Morresi, S. Mietke, R. Matzdorf, and R. Claessen, Phys. Rev. Lett. **107**, 165702 (2011).
[23] R. Heimbuch, M. Kuzmin, and H. J. W. Zandvliet, Nat. Phys. **8**, 697 (2012).
[24] C. Blumenstein, S. Meyer, S. Mietke, J. Schäfer, A. Bostwick, E. Rotenberg, R. Matzdorf, and R. Claessen, J. Phys.: Condens. Matter **25**, 014015 (2013).
[25] S. Meyer, L. Dudy, J. Schäfer, C. Blumenstein, P. Höpfner, T. E. Umbach, A. Dollinger, X. Y. Cui, L. Patthey, and R. Claessen, Phys. Rev. B **90**, 125409 (2014).
[26] J. Park, K. Nakatsuji, T.-H. Kim, S. K. Song, F. Komori, and H. W. Yeom, Phys. Rev. B **90**, 165410 (2014).
[27] F. Bechstedt, *Principles of Surface Physics* (Springer, Berlin, 2003).
[28] M. C. Gallagher, S. Melnik, and D. Mahler, Phys. Rev. B **83**, 033302 (2011).
[29] F. Krok, M. R. Kaspers, A. M. Bernhart, M. Nikiel, B. R. Jany, P. Indyka, M. Wojtaszek, R. Möller, and C. A. Bobisch, Beilstein J. Nanotech. **5**, 1463 (2014).
[30] T. Lichtenstein, H. Teiken, H. Pfnür, J. Wollschläger, and C. Tegenkamp, Surf. Sci. **632**, 64 (2015).
[31] S. Sauer, F. Fuchs, F. Bechstedt, C. Blumenstein, and J. Schäfer, Phys. Rev. B **81**, 075412 (2010).
[32] S. López-Moreno, A. H. Romero, A. Muñoz, and U. Schwingenschlögl, Phys. Rev. B **81**, 041415 (2010).
[33] C.-Y. Niu and J.-T. Wang, Solid State Commun. **151**, 655 (2011).
[34] S. Meyer, T. E. Umbach, C. Blumenstein, J. Schäfer, R. Claessen, S. Sauer, S. J. Leake, P. R. Willmott, M. Fiedler, and F. Bechstedt, Phys. Rev. B **85**, 235439 (2012).
[35] P. Hohenberg and W. Kohn, Phys. Rev. **136**, B864 (1964).
[36] W. Kohn and L. J. Sham, Phys. Rev. **140**, A1133 (1965).
[37] J. P. Perdew and A. Zunger, Phys. Rev. B **23**, 5048 (1981).
[38] J. P. Perdew, K. Burke, and M. Ernzerhof, Phys. Rev. Lett. **77**, 3865 (1996).

[39] G. Kresse and J. Furthmüller, Comput. Mat. Sci **6**, 15 (1996).
[40] J. P. Perdew, A. Ruzsinszky, G. I. Csonka, O. A. Vydrov, G. E. Scuseria, L. A. Constantin, X. Zhou, and K. Burke, Phys. Rev. Lett. **100**, 136406 (2008).
[41] G. Kresse and D. Joubert, Phys. Rev. B **59**, 1758 (1999).
[42] J. Klimeš, D. R. Bowler, and A. Michaelides, Phys. Rev. B **83**, 195131 (2011).
[43] H. J. Monkhorst and J. D. Pack, Phys. Rev. B **13**, 5188 (1976).
[44] F. Bechstedt, *Many-body Approach to Electronic Excitations* (Springer, Berlin, 2015).
[45] M. S. Hybertsen and S. G. Louie, Phys. Rev. B **34**, 5390 (1986).
[46] M. Laubscher, S. Küfner, P. Kroll, and F. Bechstedt, J. Phys.: Condens. Matter **27**, 405302 (2015).
[47] J. Tersoff and D. R. Hamann, Phys. Rev. B **31**, 805 (1985).
[48] K. Yaji, R. Yukawa, S. Kim, Y. Ohtsubo, P. L. Fèvre, F. Bertran, A. Taleb-Ibrahimi, I. Matsuda, K. Nakatsuji, and F. Komori arXiv:1602.05284.